

First-principles modeling of three-body interactions in highly compressed solid helium

Claudio Cazorla^{1,*} and Jordi Boronat^{2,†}

¹*School of Materials Science and Engineering, UNSW Australia, Sydney NSW 2052, Australia
Integrated Materials Design Centre, UNSW Australia, Sydney NSW 2052, Australia*

²*Departament de Física i Enginyeria Nuclear, Universitat Politècnica de Catalunya,
Campus Nord B4-B5, E-08034, Barcelona, Spain**

We present a new set of three-body interaction models based on the Slater-Kirkwood (SK) potential that are suitable for the study of the energy, structural and elastic properties of solid ^4He at high pressure. Our *effective* three-body potentials are obtained from the fit to total energies and atomic forces computed with the van der Waals density functional theory method due to Grimme, and represent an improvement with respect to previously reported three-body interaction models. In particular, we show that some of the introduced SK three-body potentials reproduce closely the experimental equation of state and bulk modulus of solid helium up to a pressure of ~ 60 GPa, when used in combination with standard pairwise interaction models in diffusion Monte Carlo simulations. Importantly, we find that recent predictions reporting a surprisingly small variation of the kinetic energy and Lindeman ratio on quantum crystals under increasing pressure are likely to be artifacts deriving from the use of incomplete interaction models. Also, we show that the experimental variation of the shear modulus, C_{44} , at pressures $0 \leq P \leq 25$ GPa can be quantitatively described by the new set of SK three-body potentials. At higher compression, however, the agreement between our C_{44} calculations and experiments deteriorates and thus we argue that higher order many-body terms in the expansion of the atomic interactions probably are necessary in order to better describe elasticity in very dense solid ^4He .

PACS numbers: 67.80.-s,02.70.Ss,67.40.-w

I. INTRODUCTION

The electronic structure of a single ^4He atom is among the simplest in the periodic table of elements. Likewise, the atomic interactions in liquid and solid helium can be reproduced accurately with simple analytical functions that solely depend on the distance between particles taken in pairs. Examples of successful ^4He - ^4He interaction models include the Lennard-Jones and Aziz-type semiempirical potentials.¹⁻³ Yet, under conditions of large pressures and strain deformations the interparticle interactions become more complex due to the strong electronic repulsion experienced by neighboring atoms. Consequently, pairwise potentials, which work reasonably well under near-equilibrium conditions, turn out to be unreliable. This is, for instance, the case of the Aziz-II potential,³ which at high pressure provides too repulsive atomic forces and a significant overestimation of the ^4He molar volume and bulk modulus.⁴

A recently proposed straightforward way to correct for such modeling drawbacks consists in modifying the repulsive part of standard pairwise potentials by means of an exponential attenuation factor.⁵ This possibility has already been explored in highly compressed solid ^4He ⁶ and molecular hydrogen⁷ with quantum Monte Carlo simulations, producing equations of state which are in very good agreement with experiments. Nevertheless, the use of modified pairwise potentials in very dense crystals poses a series of issues and open questions. For instance, a surprisingly small variation of the kinetic energy upon increasing pressure have been reported in works [6] and [7], and, owing to the lack of experimental data in the ther-

modynamic regime of interest, it remains to be demonstrated whether such predictions can be fully ascribed to genuine quantum nuclear effects. Also, pairwise potentials are in general not recommended for the study of elasticity in hcp crystals at high pressure since they inevitably lead to null values of the Cauchy discrepancy (defined as the difference between the two elastic constants C_{12} and C_{44}), in contrast to what is observed in experiments.⁸⁻¹¹

An alternative route to improve the description of quantum solids under extreme stress-strain conditions is to consider higher order terms, beyond pairwise additivity, in the approximation to the atomic interactions. In this context, several three-body interatomic models have already been proposed like, for instance, the Axilrod-Teller (AT), Bruch-McGee (BM), and Cohen-Murrel (CM) potentials.^{2,12,13} However, improvements resulting from the use of those three-body interaction models so far have been reported to be only marginal. For instance, three decades ago Loubeyre claimed, based on the outcomes of self-consistent phonon and classical Monte Carlo simulations, that the three-body BM interaction could bring into good agreement calculations and experiments performed on the equation of state of solid helium up to ~ 60 GPa.¹⁴ However, Chang *et al.*¹⁵ have shown more recently that when either the BM or CM three-body potentials are considered in quantum Monte Carlo simulations the resulting ^4He molar volumes are significantly underestimated, already at few GPa. Similar discouraging results have been reported also by other authors who have employed analogous three-body interaction models.¹⁶⁻¹⁸

In this article, we present new work done on the modeling of three-body interactions in highly compressed solid helium up to pressures of ~ 160 GPa. We introduce a new set of *effective* potentials based on the Slater-Kirkwood (SK) function,¹² that are obtained from the fits to *ab initio* energies and atomic forces calculated with the van der Waals corrected density functional theory method due to Grimme (DFT-D2).¹⁹ We show that an overall improved description of the energy, elastic and structural properties of solid helium can be achieved with some of the introduced SK three-body interatomic potentials, when used in combination with pairwise potentials in quantum Monte Carlo simulations. Our work also brings new insight into the physics of quantum crystals at high pressure. For instance, we show that previously reported small variations of the kinetic energy, E_k , and Lindeman ratio, γ , in solid helium under pressure⁶ are likely to be artifacts deriving from the use of incomplete atomic interaction models. Moreover, we quantify the role of quantum nuclear effects on the estimation of the shear modulus, C_{44} , and conclude that they become secondary when pressure is raised. Finally, at $P \sim 25$ GPa we find that the agreement between our C_{44} results and experiments starts to worsen. Therefore, we argue that higher order many-body terms in the expansion of the atomic interactions probably are necessary in order to describe elasticity in dense solid helium more accurately.

The organization of this article is as follows. In the next section, we outline the employed computational methods and provide the technical details in our calculations. In Sec. III, we explain the fitting strategy that we have followed to obtain the new set of *effective* three-body interaction models. Next, we present our results on the equation of state, kinetic energy, and structural and elastic properties in solid helium, together with some discussion. Finally, we summarize our main findings in Sec. V.

II. COMPUTATIONAL METHODS

We used the density functional theory method including van der Waals corrections due to Grimme¹⁹ to compute the interactions and forces between helium atoms in the hexagonal close package (hcp) crystal structure, from equilibrium up to a pressure of ~ 160 GPa. The details of our *ab initio* DFT-D2 calculations can be found in elsewhere,⁶ hence we highlight here only the main technical features. We must note that despite other more advanced methods than the DFT-D2 approach could in principle provide a more accurate description of the van der Waals forces,^{20,21} recent DFT-D2 calculations on the equation of state and bulk modulus in highly compressed helium have demonstrated very good agreement with the experiments (that is, essentially due to the secondary role played by the long-range dispersive interactions at high pressure).⁶ For our present fitting potential purposes, therefore, the DFT-D2 method can be regarded

as fairly adequate, as it will be further demonstrated in Sec. IV.

We found several *effective* three-body interaction models based on the Slater-Kirkwood (SK) potential¹² that, when used in combination with the pairwise Aziz-II potential³ (hereafter denoted as V_2), reproduced very closely the obtained DFT-D2 results. The details of our fitting strategy are comprehensively explained in Sec. III. We must acknowledge that implicit to our modeling strategy there is a certain arbitrariness in the definition of the atomic three-body forces. Actually, we assume here that the two-body interactions in solid helium are completely described by the Aziz-II potential³ and that anything that is missing on it, as deduced from the comparison to the DFT-D2 results, can be regarded as “three-body”. In order to exactly determine the form and magnitude of the three-body interactions in the crystal, one should rather perform a series of intensive *ab initio* supermolecular calculations involving a large number of dimer and trimer configurations (see, for instance, works [22] and [23] by Cencek *et al.*). Following such a sophisticated quantum chemistry approach, however, is out of the scope of the present work. In order to avoid possible misunderstandings on this point, we will refer to the set of introduced SK parametrisations as “*effective* three-body potentials” throughout the text.

Finally, we performed diffusion Monte Carlo (DMC) calculations in which the new *effective* three-body interaction models were employed to estimate the energy, structural, and elastic properties of solid helium under pressure. Next, we explain the specific implementation of the DFT-D2 and DMC methods in our work.

A. Density functional theory

We chose the generalized gradient approximation to density functional theory proposed by Perdew, Burke, and Ernzerhof (GGA-PBE),²⁴ as is implemented in the VASP package.²⁵ Van der Waals interactions were taken into account by adding an attractive energy term to the exchange-correlation energy of the form $E_{\text{disp}} = -\sum_{i,j} C_6/r_{ij}^6$ (where indexes i and j label different particles, C_6 is a constant, and a damping factor is introduced at short distances to avoid divergences).^{19–21} The projector-augmented-wave technique^{26,27} was employed to represent the core electrons since this approach has been shown to provide very accurate total energies and is computationally very efficient.^{28,29} The electronic wave functions were represented in a plane-wave basis truncated at 500 eV, and for integrations within the first Brillouin zone (BZ) we employed dense Γ -centered k -point grids of $14 \times 14 \times 14$. By using these parameters we obtained interaction energies that were converged to within 5 K per atom. Geometry relaxations were performed by using a conjugate-gradient algorithm that kept the volume of the unit cell fixed and permitted variations of its shape. The imposed tolerance on the atomic forces was

0.005 eV·Å⁻¹. With such a DFT-D2 setup we calculated the total energy and shear modulus in solid ⁴He in the volume interval $3 \leq V \leq 16 \text{ \AA}^3/\text{atom}$.

Additionally, we computed the vibrational phonon spectrum in solid ⁴He at eight different volumes by means of the “direct approach”. In the direct approach the force-constant matrix is directly calculated in real-space by considering the proportionality between atomic displacements and forces when the former are sufficiently small.^{30–32} In this case, large supercells have to be simulated in order to guarantee that the elements of the force-constant matrix have all fallen off to negligible values at their boundaries, a condition that follows from the use of periodic boundary conditions.³³ Once the force-constant matrix is obtained, we Fourier-transform it to obtain the phonon spectrum at any q -point. The quantities with respect to which our DFT-D2 phonon calculations need to be converged are the size of the supercell and atomic displacements, and the numerical accuracy in the atomic forces. The following settings were found to fulfill our convergence requirement of correct zero-point energy corrections to within 5 K/atom:^{6,30} $4 \times 4 \times 3$ supercells (that is, 48 repetitions of the hcp unit cell containing a total of 96 atoms), and atomic displacements of 0.02 Å. Regarding the calculation of the atomic forces with VASP, we found that the density of k -points had to be increased slightly with respect to the value used in the energy calculations (i.e., from $14 \times 14 \times 14$ to $16 \times 16 \times 16$) and that computation of the non-local parts of the pseudopotential contributions needed to be performed in reciprocal, rather than real, space.

B. Diffusion Monte Carlo

In our DMC simulations, we used a guiding wave function, Ψ_{SNJ} , that accounts simultaneously for the atomic periodicity and Bose-Einstein quantum symmetry in ⁴He crystals. This model wave function is expressed as³⁴

$$\Psi_{\text{SNJ}}(\mathbf{r}_1, \dots, \mathbf{r}_N) = \prod_{i < j}^N f(r_{ij}) \prod_{J=1}^N \left(\sum_{i=1}^N g(r_{iJ}) \right), \quad (1)$$

where indexes $\{i, j\}$ and J run over particles and perfect lattice positions, respectively. In previous works we have shown that Ψ_{SNJ} provides an excellent description of the ground-state properties of bulk hcp ⁴He and other similar quantum systems.^{34–37} The correlation factors in Eq. (1) were expressed in the McMillan, $f(r) = \exp[-1/2 (b/r)^5]$, and Gaussian, $g(r) = \exp[-1/2 (ar^2)]$, forms. Parameters a and b were optimized at each density point by using the variational Monte Carlo (VMC) method. For instance, at $\rho = 0.06 \text{ \AA}^{-3}$ we obtained $b = 2.94 \text{ \AA}$ and $a = 3.21 \text{ \AA}^{-2}$, and at $\rho = 0.33 \text{ \AA}^{-3}$, $b = 1.84 \text{ \AA}$ and $a = 29.08 \text{ \AA}^{-2}$. We note that our choice of the guiding function was motivated by an interest in studying the possible effects of

quantum atomic exchanges on the energetic and elastic properties of dense helium. Nevertheless, we realised through the direct comparison to results obtained with non-symmetric wave function models in analogous DMC simulations,⁶ that such effects can be totally neglected in practice.

The technical parameters in our calculations were set to ensure convergence of the total energy per particle to less than 0.5% of its value. The average population of walkers was 10^3 and the length of the imaginary time-step ($\Delta\tau$) 10^{-4} K^{-1} (the adequacy of these settings for the study of highly compressed quantum crystals has already been demonstrated in work [6], see Figure 3 therein). We used simulation cells containing 180 atoms. Numerical bias stemming from the finite size of the simulation box were minimised by following the variational correction approach explained in works [4] and [6]. Statistics were accumulated over 10^5 DMC steps performed after system equilibration, and the approximation used for the short-time Green’s function, $e^{-\hat{H}\tau}$, was accurate to second order in $\Delta\tau$.^{2,38} The computational strategy that we followed to calculate the shear modulus C_{44} is the same than explained in Refs. [39–41].

III. FITTING STRATEGY AND THE EFFECTIVE THREE-BODY POTENTIAL

Our three-body potential matching algorithm^{42–44} is based on a least square fit to the DFT-D2 reference data, that consists of total energies and atomic forces. The objective function to be minimized is given by

$$\chi^2 = \omega_E \times \sum_i^N \frac{(E_i^{\text{FF}} - E_i^{\text{DFT}})^2}{\sum_j^N (E_j^{\text{DFT}} - \langle E^{\text{DFT}} \rangle)^2} + \omega_F \times \sum_i^N \frac{\sum_{l,\alpha}^{n,3} (F_{l\alpha,i}^{\text{FF}} - F_{l\alpha,i}^{\text{DFT}})^2}{\sum_{l,\alpha,j}^{n,3,N} (F_{l\alpha,j}^{\text{DFT}} - \langle F^{\text{DFT}} \rangle)^2}, \quad (2)$$

where $N = 16$ is the number of reference configurations, $n = 96$ the number of particles on each configuration, and ω_E and ω_F a weight assigned to the energy, E , and force, F , contributions to χ^2 , respectively. With this definition of the objective function we ensure that despite different magnitudes are expressed in different units all them are normalized and contribute equally to χ^2 . Subscripts “DFT” and “FF” refer to the DFT-D2 and classical potential results, respectively.

The set of reference configurations in our fit comprised the 16 structures used in the calculation of the ⁴He vibrational phonon spectra in the interval $3 \leq V \leq 16 \text{ \AA}^3/\text{atom}$ by means of the “direct approach” (see Sec. II A).^{30–32} Those atomic arrangements were generated by taking the relaxed hcp lattice supercells ($P6_3/mmc$, space group 194) at 8 different volumes and displacing one of the atoms sitting in an inequivalent d Wyckoff position a distance of 0.02 Å first along the

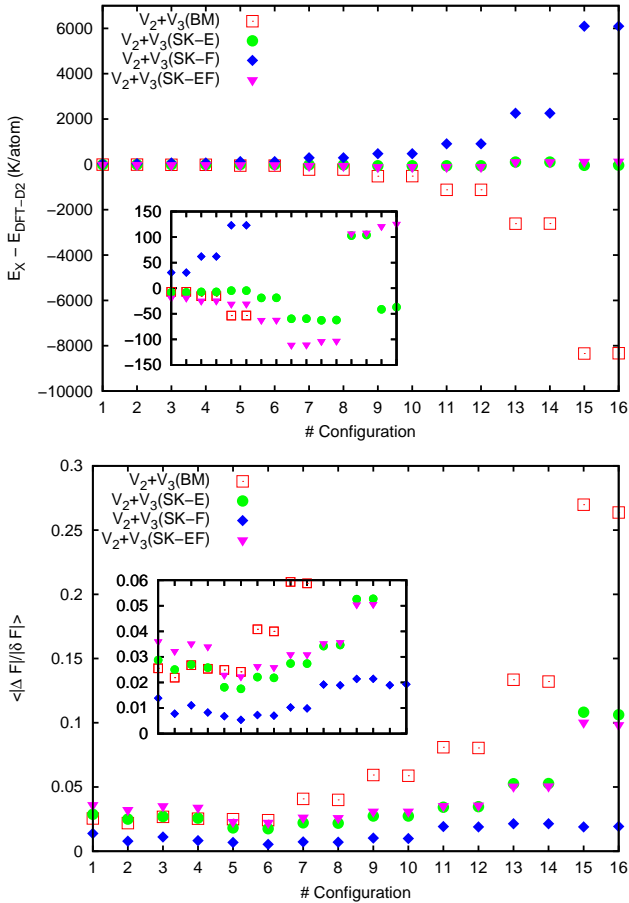


FIG. 1. (Top) Energy differences between the DFT-D2 method and V_3 potentials calculated on a reference set of 16 configurations (see text). Details are magnified in the inset. (Bottom) Results of our fit obtained in the case of the atomic forces. ΔF stands for the difference in the atomic forces between the DFT-D2 method and many-body potentials, δF for the variance of the atomic forces computed with the DFT-D2 method, and $\langle \dots \rangle$ for the average performed over particles and Cartesian components.

$\frac{1}{2}\hat{x} - \frac{\sqrt{3}}{2}\hat{y}$ direction (where $\hat{x}, \hat{y}, \hat{z}$ represent the normalised Cartesian vectors), and then along \hat{z} (that is, we created two different atomic configurations at each volume). The reason for our choice was that we wanted to reproduce simultaneously the energy and elastic properties in highly compressed solid ^4He . In fact, the atomic forces are defined as minus the first derivative of the total energy with respect to the atomic positions, whereas the elastic constants involve the second derivative of the total energy with respect to strain deformations. In spite of this apparent disconnection, atomic forces and elastic constants are indirectly related by the corresponding spectrum of vibrational phonon frequencies. Namely, on one side, phonons can be calculated from the variation of the atomic forces upon the displacement of atoms away from their equilibrium positions, and, on the other side, elastic constants can be estimated from the slope of spe-

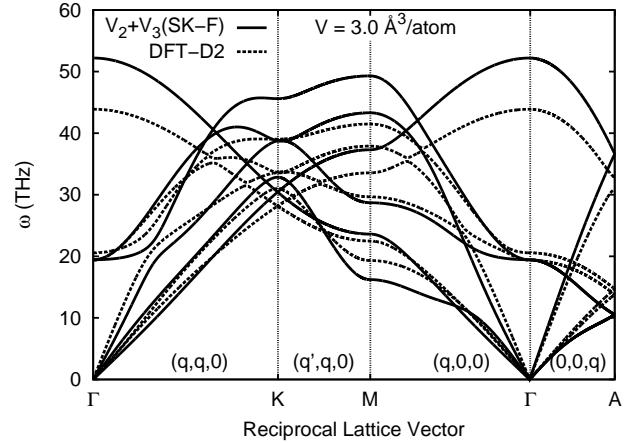


FIG. 2. Phonon spectrum calculated with the DFT-D2 method (dashed lines) and the $V_2 + V_3$ (SK-F) interaction model (solid lines), which was determined considering only the atomic forces in the corresponding fit (see text), at $P \sim 160$ GPa. We note that in the present notation 1 THz is equal to 4.31566554 meV .

cific acoustic branches in the vicinity of the Γ point in reciprocal space (that is, in the $q \rightarrow 0$ limit). Therefore, even though we did not explicitly consider second derivatives in our definition of the objective function χ^2 , we expected to achieve an acceptable description of elasticity in solid helium. We shall come back to this point later on this section.

The classical potential adopted in this study, denoted as “FF” in Eq. 2, is given by $U_{\text{pot}} = V_2 + V_3$, where V_2 represents the pairwise Aziz-II interaction model³ and V_3 the three-body Slater-Kirkwood (SK) potential function given by¹²

$$V_3(r_{ij}, r_{ik}, r_{jk}) = \left[\frac{\nu}{r_{ij}^3 r_{ik}^3 r_{jk}^3} - A \exp(-\alpha[r_{ij} + r_{ik} + r_{jk}]) \right] \times (1 + 3 \cos \phi_i \cos \phi_j \cos \phi_k), \quad (3)$$

where $r_{ij} = |\mathbf{r}_i - \mathbf{r}_j|$, and ϕ_i, ϕ_j , and ϕ_k , are the interior angles of the triangle formed by the atoms labelled i, j , and k . V_3 is an attractive potential term representing triple dipole and three-body exchange interactions. Parameters ν, A , and α were varied during the minimization of the objective function χ^2 (see Eq. 2). For this, we used a quadratic polynomial interpolation line-search with the directions found using the Broyden-Fletcher-Goldfarb-Shanno (BFGS) formula.⁴⁵ The gradient of the objective function was calculated analytically since otherwise numerical bias developed that impeded convergence. Actually, the typical size of the involved atomic forces is very small, of the order of $0.01 - 0.1 \text{ eV/\AA}$, hence they needed to be calculated very precisely. The minimizations were stopped when all the gradients of the objective function in absolute value were smaller than 10^{-5} . Typically, this was achieved within ~ 100 minimization loops when starting from a reasonable initial guess of the ν, A ,

and α parameters (e.g., the original values proposed by Bruch and McGee [12]).

Table I shows the values of the parameters obtained in our V_3 fits, in which we considered three different possibilities based on the choice of the relative energy and forces weights: (1) $\omega_E = 1$ and $\omega_F = 0$, hereafter denoted as $V_3(\text{SK-E})$, (2) $\omega_E = 0$ and $\omega_F = 1$, $V_3(\text{SK-F})$, and (3) $\omega_E = 0.5$ and $\omega_F = 0.5$, $V_3(\text{SK-EF})$. Our results differ appreciably from the original values proposed by Bruch and McGee [which hereafter are denoted as $V_3(\text{BM})$]. For instance, ν becomes negative when the energies are taken into account in the fit, and A and α systematically turn out to be larger.

In Figure 1, we demonstrate the quality of our fits by plotting the energies and forces calculated on each reference configuration. For comparison purposes, we also enclose the results obtained with the original $V_3(\text{BM})$ potential (i.e., with the potential function $U_{\text{pot}} = V_2 + V_3$). For the sake of simplifying the notation, we only indicate the three-body part in the corresponding *effective* potential. This convention will be adopted throughout the text if not stated otherwise. As is appreciated in the figure, $V_3(\text{SK-E})$ reproduces the DFT-D2 energies more closely than any other model (as expected) whereas $V_3(\text{BM})$ provides the worst description. The energies obtained with the $V_3(\text{SK-EF})$ potential can be regarded also as fairly good. As for the atomic forces, $V_3(\text{SK-F})$ produces the best results, as expected, and $V_3(\text{BM})$, again, turns out to be the less reliable. In this latter case, the forces obtained with the $V_3(\text{SK-EF})$ and, surprisingly also, $V_3(\text{SK-E})$ potentials are not too distant from the reference DFT-D2 data.

Figure 2 shows the vibrational phonon spectra obtained with the DFT-D2 method and the $V_3(\text{SK-F})$ potential in solid ^4He at the smallest considered volume (i.e., $V = 3.0\text{\AA}^3/\text{atom}$, which probably is the most challenging case to be reproduced with an *effective* potential function, see Fig. 1). We note that the agreement between the two sets of data can be regarded as fairly good. The largest differences are found on the optical branches, which correspond to the highest vibrational frequency values. The DFT-D2 acoustic phonon modes in the vicinity of the Γ point, however, are reasonably well reproduced by $V_3(\text{SK-F})$. These outcomes demonstrate that, as we suggested above, by considering the atomic forces in the definition of χ^2 in principle one can obtain a reasonable description of elasticity in the reference system.

Finally, we calculated the interaction energy of several trimer configurations for which the *exact* full-configuration-interaction (FIC) energies have been reported by Cencek *et al.* (see work [23]). The trimer configurations consist of three equilateral triangles of sides $l = 3.7042, 2.9634, \text{ and } 2.1167\text{\AA}$, respectively. The interaction energies obtained with the SK-E, SK-EF and BM potentials (i.e., by using the potential function $U_{\text{pot}} = V_2 + V_3$) and considering the atomic positions fixed, are enclosed in Table II. As is appreciated therein,

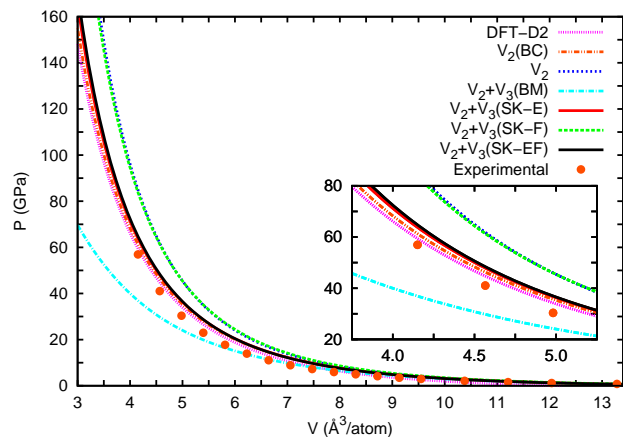


FIG. 3. Zero-temperature equation of state calculated in helium with the DFT-D2 and DMC methods. In the DMC case, different pairwise and *effective* three-body interaction models have been employed. Experimental data from Ref. [46] are shown for comparison. *Inset*: The high- P region in the $P(V)$ curves are magnified in order to appreciate better the differences.

the $V_3(\text{SK-E})$ results are in closer agreement with the FIC benchmarks in the two trimer configurations with larger side lengths. In those two cases, the $V_3(\text{SK-E})$ energies present the largest discrepancies with respect to the reference results although these are still reasonably small (i.e., $\sim 0.6\%$). In the trimer configuration with the smallest side length, both the SK-E and SK-EF potentials overestimate the corresponding interaction energy by ~ 20 K whereas the BM function underestimates it by approximately the same quantity. This last outcome is consistent with the results shown in Fig. 1 for bulk solid helium. Unfortunately, we have not found in the literature FIC or similar benchmark energy results for helium trimers with interatomic distances as small as considered in this work (that is, $l \sim 1.6\text{\AA}$), hence a further comparative V_3 analysis based on the interaction energy of few-body systems is not possible at the moment.

IV. RESULTS AND DISCUSSION

A. Equation of state

Figure 3 shows the results of our calculations on the equation of state, $P(V)$, of solid helium together with the experimental data found in work [46]. The DFT-D2 series was obtained with the *ab initio* methods described in Sec. II A, including quantum zero-point energy corrections. The other results were obtained with the diffusion Monte Carlo (DMC) method by using several *effective* interaction models, as explained in Sec. II B and elsewhere [6]. Labels “ V_2 ” and “ $V_2(\text{BC})$ ” stand respectively for the pairwise potential due to Aziz³ and a modified version of the former that we have recently introduced

	ν (K $\cdot\sigma^9$)	A (K)	α (σ^{-1})
V_3 (BM) [12]	0.3270	9 676 545.53	4.9480
V_3 (SK-E)	-0.4910	14 754 161.38	5.6128
V_3 (SK-F)	1.4029	12 863 029.73	5.8273
V_3 (SK-EF)	-1.1364	29 189 436.37	6.0691

TABLE I. Three-body potential parameters of the original Bruch-McGee model, V_3 (BM), and the new SK *effective* potentials introduced in the present work. The V_3 (SK-E) parametrisation has been obtained by considering exclusively DFT-D2 energies on the fit [$\omega_E = 1$, $\omega_F = 0$], the V_3 (SK-F) the atomic forces [$\omega_E = 0$, $\omega_F = 1$], and V_3 (SK-EF) a combination of *ab initio* energies and atomic forces [$\omega_E = 0.5$, $\omega_F = 0.5$] (see text). It is noted that $\sigma \equiv 2.556$ Å.

	Trimer 1 (3.7042 Å)	Trimer 2 (2.9634 Å)	Trimer 3 (2.1167 Å)
V_3 (BM) [12]	-13.8298	-33.1717	804.95
V_3 (SK-E)	-13.8642	-33.0898	842.05
V_3 (SK-EF)	-13.8953	-33.2841	843.68
Exact [23]	-13.8510	-33.1026	821.44

TABLE II. Interaction energy calculated in different trimer configurations consisting of equilateral triangles (the corresponding side lengths are indicated within parentheses). Energies are expressed in Kelvin.

in work [6]. The DMC (DFT-D2) calculations were performed at 12 (8) different volumes spanned in the interval $3 \leq V \leq 16$ Å³/atom. In each case, the resulting total energies were fitted to a third order Birch-Murnaghan equation of the form^{47,48}

$$E(V) - E_0 = \frac{3}{2} V_0 B_0 \times \left[-\frac{\chi}{2} \left(\frac{V_0}{V} \right)^2 + \frac{3}{4} (1 + 2\chi) \left(\frac{V_0}{V} \right)^{(4/3)} - \frac{3}{2} (1 + \chi) \left(\frac{V_0}{V} \right)^{(2/3)} + \frac{1}{2} \left(\chi + \frac{3}{2} \right) \right], \quad (4)$$

where $B_0 = V_0 \frac{d^2 E}{dV^2}$ is the value of the bulk modulus at the equilibrium volume V_0 , $\chi = \frac{3}{4} (4 - B'_0)$ with $B'_0 = (dB_0/dP)$, and all the derivatives are calculated at zero pressure. For reproducibility purposes, we enclose the V_0 , B_0 , and B'_0 parameters obtained in all our fits in Table III.

Very good agreement is obtained between our DFT-D2 results and experiments. This outcome justifies in part

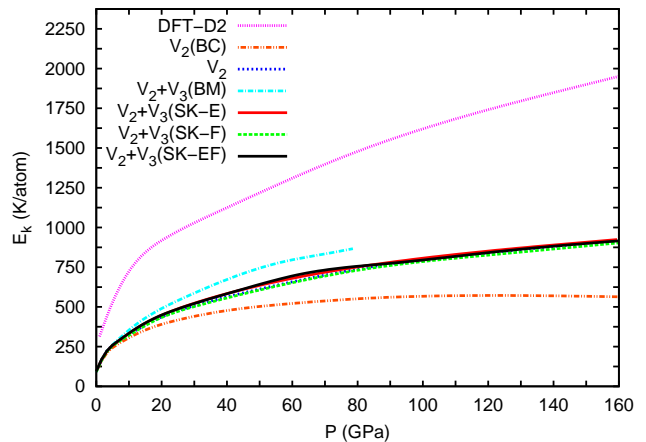


FIG. 4. Atomic kinetic energy calculated in ⁴He with the DFT-D2 and DMC methods and expressed as a function of pressure. In the DMC case, different pairwise and *effective* three-body interaction models have been considered for the description of the atomic interactions.

	V_0 (\AA^3)	B_0 (eV/ \AA^3)	B'_0
DFT – D2	12.23	0.0398	3.9648
V_2 (BC)	15.68	0.0166	4.1144
V_2	16.61	0.0115	4.8829
$V_2 + V_3$ (BM)	15.68	0.0181	3.6722
$V_2 + V_3$ (SK-E)	15.84	0.0165	4.1854
$V_2 + V_3$ (SK-F)	16.58	0.0130	4.6709
$V_2 + V_3$ (SK-EF)	15.85	0.0158	4.2463

TABLE III. Parameters corresponding to the fit of our equation of state results to Birch-Murnaghan functions, see Eq. (4), as obtained with different computational approaches. In the DMC case, different pairwise and *effective* three-body potentials have been considered for the description of the interatomic forces.

our choice of the DFT-D2 results as reference data in modeling of the many-body interactions. Likewise, the $P(V)$ curves obtained with the V_2 (BC), V_3 (SK-E), and V_3 (SK-EF) potentials are also very close to the observations. We notice that the V_2 (BC) model introduced in Ref. [6] was constructed to reproduce the equation of state calculated with the DFT-D2 method and that the good agreement displayed in Fig. 3 is not a new result. Contrarily, the V_2 , V_3 (BM), and V_3 (SK-F) potentials provide a poor description of the variation of the volume under pressure. In particular, we find that the V_3 (BM) potential systematically underestimates V at pressures equal or larger than 20 GPa, in accordance with previous results reported by other authors.^{15,16} Meanwhile, the V_2 and V_3 (SK-F) interaction models significantly overestimate the same quantity at pressures also close to or larger than 20 GPa. In this latter case, we notice a surprising resemblance between the two calculated $P(V)$ curves.

The main conclusion emerging from this part of our study is that the new V_3 (SK-E) and V_3 (SK-EF) *effective* three-body potentials reproduce very accurately the equation of state of solid helium up to a pressure of ~ 60 GPa (and possibly beyond). To the best of our knowledge, such a good agreement between theory and experiments has not been reported before for any known V_3 potential in solid ^4He (see work [15]).

B. Kinetic energy

Our kinetic energy, E_k , results are shown in Fig. 4. In our DFT-D2 calculations, the kinetic energy was estimated within the quasiharmonic approximation through

the expression

$$E_k^{\text{qh}}(V) = \frac{1}{N_q} \sum_{qs} \frac{1}{2} \hbar \omega_{qs}(V), \quad (5)$$

where ω_{qs} are the vibrational phonon frequencies in the crystal calculated at wave vector \mathbf{q} and phonon branch s , which depend on the volume, and N_q the total number of wave vectors used for integration within the first Brillouin zone (see Sec. II A and works [6 and 30]). E_k^{qh} usually is referred to as the “zero-point energy” (ZPE) and in many computational studies turns out to be crucial for predicting accurate solid-solid phase transitions.^{31,32,48} Regarding our DMC calculations, we computed first the *exact* potential energy, E_p , by means of the pure estimator technique^{49,50} and subsequently obtained the *exact* kinetic energy by subtracting E_p to the corresponding total energy. In all the cases, spline interpolations were applied to the calculated data points in order to obtain smooth P -dependent energy curves (lines in Fig. 4).

As is appreciated in the figure, the DFT-D2 results differ enormously from the rest of E_k series obtained with pairwise and *effective* three-body potentials in our DMC simulations. At the highest analysed pressure, for instance, the DFT-D2 kinetic energy is a factor of two larger than the obtained DMC value. Given the lack of experimental data in the thermodynamic regime of interest, we can not rigorously conclude which type of calculation is providing the most realistic description. Nevertheless, we think that the DFT-D2 results are overestimating E_k severely because they have been obtained using the quasiharmonic approximation. In fact, it has been already demonstrated that the quasiharmonic approximation is not appropriate for studying crystals that behave much more classically than solid helium like, for instance,

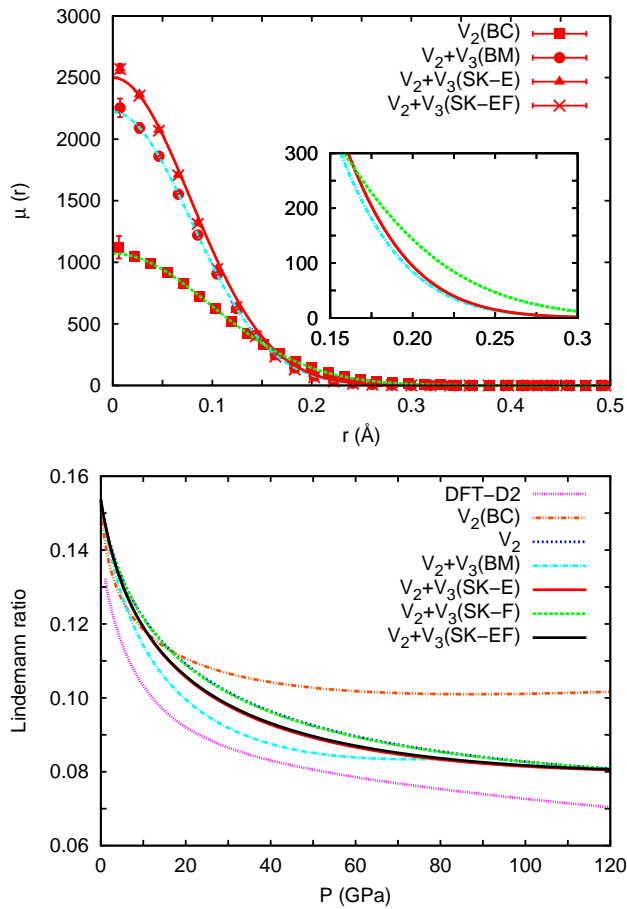


FIG. 5. (*Top*) Atomic density profile around the perfect lattice positions calculated with the DMC method considering different pairwise and *effective* three-body interaction models ($V = 3.0 \text{ \AA}^3/\text{atom}$). Solid lines correspond to Gaussian curves fitted to the results. The corresponding tails are magnified in the inset in order to better appreciate the differences. (*Bottom*) Lindeman ratio calculated in solid ^4He with the DFT-D2 and DMC methods, expressed as a function of pressure.

molecular hydrogen,^{51–53} ammonia,^{54,55} and some alkali metals.^{56,57} It is worth noticing here that although the quasiharmonic DFT-D2 approach can produce equations of state that are in very good agreement with experiments (as it has been shown in Sec. IV A), the accompanying ZPE corrections have a lot of margin for error since at high P these are always several orders of magnitude smaller than the energy of the perfect crystal lattice. We shall comment again on this point in the next paragraph.

It is interesting to analyse the differences found between the (full quantum) DMC results obtained with different pairwise and *effective* three-body potential models. The $V_2(\text{BC})$ curve shows a plateau around 550 K at pressures equal and beyond ~ 80 GPa. In a recent work,⁶ we identified such an infinitesimal variation in the kinetic energy with the presence of extreme quantum nuclear effects. However, calculations performed with the new set of *effective* three-body potentials introduced in this

work bring new light into our previous interpretation of the $V_2(\text{BC})$ results. As is observed in Fig. 4, the $V_3(\text{SK-E})$, $V_3(\text{SK-F})$, and $V_3(\text{SK-EF})$ curves consistently display a small but steady increase in the kinetic energy under compression. At pressures below ~ 15 GPa the pairwise and *effective* three-body interaction models roughly provide equivalent E_k results however at $P = 160$ GPa the differences between them are as large as ~ 300 K, with the V_3 potentials providing always the largest values. Several conclusions can be drawn from these results. First, although attenuated pairwise potentials based on exponential prefactors⁵ can fairly reproduce experimental $P(V)$ data,^{6,7} they are likely to introduce unwanted bias on the calculation of the kinetic energy. And second, the large E_k discrepancies observed between the DFT-D2 and V_3 results do not seem to be originated by the absence of four-, five- and so on many-body interactions in the DMC calculations. Actually, by comparing the energy curves obtained in the V_2 and $V_2 + V_3$ cases one realizes that the effect of considering *effective* three-body interactions on E_k is rather small [only in the $V_3(\text{BM})$ case those effects are not negligible, although certainly minor]. Therefore, it is reasonable to expect similar trends when eventually one would add higher order many-body terms in the description of the atomic interactions. In regard to this last point, we notice that one of the main conclusions presented in work [6], namely that the quasiharmonic DFT approach exceedingly overestimates E_k in dense ^4He , appears to be valid.

C. Structural properties

An analysis of the atomic structure in solid ^4He at high pressure will allow us to understand better the origins of the discrepancies found so far between the $V_2(\text{BC})$ and V_3 potentials. Figure 5 shows the atomic density profiles, $\mu(r)$, and Lindeman ratio, γ , calculated using the DMC method and several atomic interaction models. The $\mu(r)$ results (see top panel) were obtained at volume $V = 3.0 \text{ \AA}^3/\text{atom}$ and subsequently were fitted to Gaussian functions (solid lines in the figure). As is observed there, the $V_2(\text{BC})$ curve is noticeably broader than all the others, and its value at the origin is about 50 % of that calculated with the $V_3(\text{BM})$ potential. Meanwhile, the $V_3(\text{SK-E})$ and $V_3(\text{SK-EF})$ profiles are practically indistinguishable and slightly higher near zero than the one obtained in the $V_3(\text{BM})$ case. Clearly, the $V_2(\text{BC})$ potential produces a much larger atomic delocalization than the rest of interaction models, which is consistent with the kinetic energy results explained in the previous section.

As for the Lindeman ratio γ (see bottom panel in Fig. 5), we have estimated the corresponding dependence on pressure for each analysed potential. In the DFT-D2 case, γ was computed within the quasiharmonic approximation using the formula $9\hbar^2/8m_{\text{He}}E_k^{\text{qh}}$, see Eq. (5) and works [35 and 58]. The results obtained in the $V_2(\text{BC})$

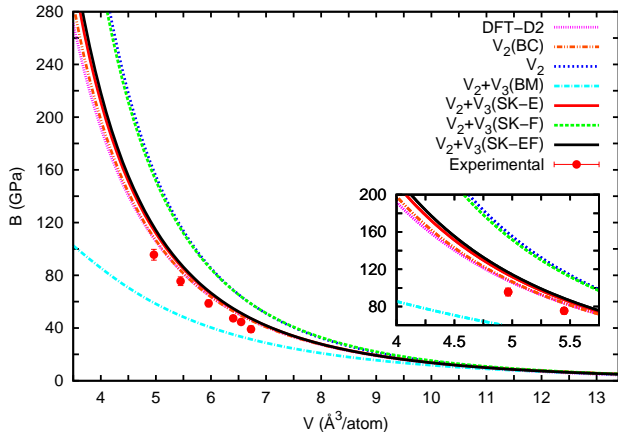


FIG. 6. Calculated bulk modulus in ${}^4\text{He}$ using the DFT-D2 and DMC methods and expressed as a function of volume. In the DMC case, different pairwise and *effective* three-body interaction models have been considered. Experimental data from work [11] are shown for comparison. *Inset*: The high- P region in the $B(P)$ curves are magnified in order to appreciate better the differences.

case are already known: a plateau around 0.10 appears at pressures larger than ~ 80 GPa.⁶ However, all the other interaction models, including V_2 and $V_3(\text{BM})$, provide much smaller values of γ at similar conditions. Moreover, the computed Lindeman ratio curves get depleted when compression is raised [with the exception of $V_3(\text{BM})$, in which γ saturates around 0.08 at pressures larger than ~ 50 GPa]. This latter trend is also observed in the DFT-D2 series, which systematically lies below the DMC predictions.

The results presented in this section show that the $V_2(\text{BC})$ potential produces an unusually large delocalization of the atoms, which is at odds with the trends realised in the rest of cases. Such a huge particle dispersion effect is the responsible for the flat kinetic energy curve appearing in Fig. 4, which is likely to be an artifact deriving from the use of exponential attenuation factors at short distances.

D. Elastic properties

In Figs. 6 and 7, we show the bulk and shear moduli, B and C_{44} respectively, calculated in solid helium under pressure. The bulk modulus was directly obtained from the Birch-Murnaghan fits explained in Sec. IV A, and in the C_{44} case spline interpolations were applied to the calculated data points in order to obtain smooth V -dependent curves.

Concerning the analysis of our $B(V)$ results, this is very much similar to the conclusions presented for the equation of state in Sec. IV A. Essentially, the DFT-D2, $V_2(\text{BC})$, $V_3(\text{SK-E})$, and $V_3(\text{SK-EF})$ curves are in good agreement with experiments whereas the V_2 , $V_3(\text{SK-F})$,

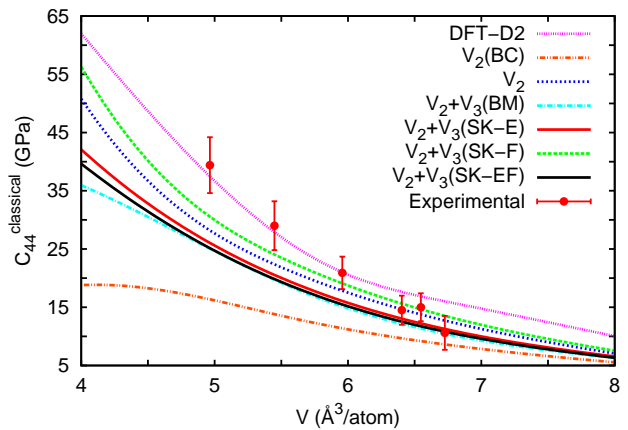


FIG. 7. Calculated shear modulus in ${}^4\text{He}$ using the DFT-D2 method and several force fields considering the atoms immobile in the perfect lattice positions. Experimental data are from work [11].

and $V_3(\text{BM})$ curves are not. In this latter case, both V_2 and $V_3(\text{SK-F})$ series are very similar and significantly overestimate the bulk modulus at small volumes. Likewise, the $V_3(\text{BM})$ potential provides unrealistically small values of $B(V)$ at large densities.

Let us now comment on the $C_{44}(V)$ results shown in Fig. 7. All the values have been obtained considering the atoms fixed on their perfect lattice positions, that is, totally neglecting likely quantum nuclear effects (hence the employed superscript). This is done for the sake of comparison since it is technically difficult to account for quantum nuclear effects in the DFT-D2 calculations in an exact manner, that is, to go beyond the quasiharmonic approximation. Nevertheless, later on this section we will show that according to our DMC simulations quantum nuclear effects become secondary on C_{44} at high pressure. As is observed in the figure, the DFT-D2 curve is in overall good agreement with the ambient temperature measurements performed by Zha and collaborators.¹¹ Again, these findings justify our choice of the benchmark data for the modeling of *effective* three-body interactions. Regarding the performance of the original three-body BM and the new SK potentials, we find that in general they reproduce quite satisfactorily the experimental data obtained at volumes larger than $\sim 5.5 \text{ \AA}^3/\text{atom}$ (i.e., $P \leq 25$ GPa). This is especially true in the $V_3(\text{SK-F})$ case where, as expected (see Sec. III), the calculated shear moduli follow closely those obtained with the DFT-D2 method. However, at volumes smaller than $\sim 5.5 \text{ \AA}^3/\text{atom}$ (i.e., $P \geq 25$ GPa) we find that the differences between the SK curves [including the $V_3(\text{SK-F})$ case], on one side, and the DFT-D2 results and experiments, on the other, become increasingly larger. We recall that the $V_3(\text{SK-E})$ and $V_3(\text{SK-EF})$ potentials provide a very good description of the equation of state and bulk modulus, whereas the $V_3(\text{SK-F})$ potential does not.

	$P(V)$	$B(V)$	$C_{44}(V)$	E_k/γ	General performance
V_2 [3]	×	×	√/×	√ (?)	Not satisfactory
$V_2(\text{BC})$ [6]	√	√	×	×	Not satisfactory
$V_2 + V_3(\text{BM})$ [12]	×	×	√/×	√ (?)	Not satisfactory
$V_2 + V_3(\text{SK-E})$	√	√	√/×	√ (?)	Overall good
$V_2 + V_3(\text{SK-F})$	×	×	√/×	√ (?)	Not satisfactory
$V_2 + V_3(\text{SK-EF})$	√	√	√/×	√ (?)	Overall good

TABLE IV. Summary of the performance of the pairwise and *effective* three-body atomic interaction models analysed in this work in describing the energy, structural, and elastic properties of solid ^4He at high pressure. Symbol \checkmark (\times) indicates correct (incorrect) description of the considered quantity, whereas \checkmark/\times means quantitatively correct up to a certain pressure. Question mark “?” denotes a certain hesitation due to lack of experimental data in the high pressure regime of interest.

This appreciation let us to conclude that is very difficult to provide simultaneously a good account of the energy and elastic properties in solid helium by using an *effective* three-body approach. Higher order many-body contributions in the description of the atomic interactions probably are necessary in order to attain an overall correct description of solid helium at high pressure. As for the pairwise potentials, V_2 performs very similarly to the $V_3(\text{SK-F})$ model, as we have also noted in the total energy (see Sec. IV A) and bulk modulus cases. The $V_2(\text{BC})$ model, however, remarkably fails in reproducing the variation of the shear modulus under pressure. Moreover, it predicts the occurrence of unrealistic mechanical instabilities (i.e., $dC_{44}/dV \approx 0$)^{59,60} at small volumes. Therefore, the use of the $V_2(\text{BC})$ potential is strongly not recommended for the simulation of solid helium at high pressure.

In order to quantify the importance of quantum nuclear effects on the calculation of the shear modulus, we carried out additional quantum DMC calculations (see Sec. II B and works [39–41] for details). To our surprise, we found that the quantum and classical shear moduli results are very similar. For instance, in the $V_3(\text{SK-F})$ case the $C_{44}^{\text{classical}} - C_{44}^{\text{quantum}}$ difference (where superscript “quantum” means calculated with the DMC method) amounts only to 2 GPa at $P \sim 50$ GPa. Similar results were obtained also in the rest of V_2 and V_3 cases. We note that the sign of the differences is always positive, thus the inclusion of quantum nuclear effects tends to lower the classical C_{44} values, although in a small fraction (i.e., $\simeq 5\%$). This last finding appears to be consistent with conclusions presented in a recent quantum Monte Carlo study by Borda *et al.*,⁶¹ in which the ideal shear strength on the basal plane of hcp ^4He was found to behave analogously than in classical solids.

V. CONCLUSIONS

In Table IV we summarise the performance of the analysed pairwise and *effective* three-body potentials in describing the energy, elastic and structural properties of solid ^4He at high pressure. A number of tips can be drawn from our results. First of all, the use of pairwise potentials in general is not recommended. These either fail to reproduce the equation of state and bulk modulus, i.e., V_2 , or the kinetic energy, and structural and elastic features, i.e., $V_2(\text{BC})$, in highly compressed quantum crystals. In this context, we urge to employ more versatile many-body interaction models. This is the case, for instance, of the new *effective* three-body BM potentials introduced in this work, which represent an improvement with respect to previously reported similar models. Overall, we recommend to consider the $V_3(\text{SK-E})$ and $V_3(\text{SK-EF})$ parametrizations in prospective simulation studies because they provide the most satisfactory general description of dense solid ^4He . Indeed, those interaction models can be safely employed, for instance, in atomistic high- P high- T simulations (either classical or quantum), which are of relevance to planetary sciences. Nevertheless, we must note that it remains a challenge to attain a precise description of elasticity at high pressure by using *effective* three-body potentials, thus in this latter case consideration of higher order many-body terms appears to be necessary.

Importantly, we have shown that the addition of *effective* three-body forces corrects for the artificially large atomic delocalization found with modified pairwise potentials based on exponential attenuation factors. Nevertheless, given the lack of structural and kinetic energy measurements performed at high pressure, we have not been able to quantify the accuracy of our γ and E_k DMC results obtained with the $V_3(\text{SK-E})$ and $V_3(\text{SK-EF})$ po-

tential models. In this regard, advanced computational studies in which both the nuclear and electronic degrees of freedom in the crystal were to be treated at the quantum level are highly desirable.

ACKNOWLEDGMENTS

This research was supported under the Australian Research Council's Future Fellowship funding scheme

(project number FT140100135), and MICINN-Spain (Grants No. MAT2010-18113, CSD2007-00041, and FIS2014-56257-C2-1-P). Computational resources and technical assistance were provided by the Australian Government through Magnus under the National Computational Merit Allocation Scheme.

* c.cazorla@unsw.edu.au

† jordi.boronat@upc.edu

¹ M. H. Kalos, M. A. Lee, and P. A. Whitlock, Phys. Rev. B **24**, 115 (1981).

² J. Boronat and J. Casulleras, Phys. Rev. B **49**, 8920 (1994).

³ R. A. Aziz, F. R. W. McCourt, and C. C. K. Wong, Mol. Phys. **61**, 1487 (1987).

⁴ C. Cazorla and J. Boronat, J. Phys.: Condens. Matter. **20**, 015223 (2008).

⁵ M. Moraldi, J. Low Temp. Phys. **168**, 275 (2012).

⁶ C. Cazorla and J. Boronat, Phys. Rev. B **91**, 024103 (2015).

⁷ T. Omiyinka and M. Boninsegni, Phys. Rev. B **88**, 024112 (2013).

⁸ D. C. Wallace, *Thermodynamics of Crystals* (Wiley, New York, 1972).

⁹ E. Pechenik, I. Kelson, and G. Makov, Phys. Rev. B **78**, 134109 (2008).

¹⁰ Y. A. Freiman, S. M. Tretyak, A. Grechnev, A. F. Goncharov, J. S. Tse, D. Errandonea, H.-K. Mao, and R. J. Hemley, Phys. Rev. B **80**, 094112 (2009).

¹¹ C.-S. Zha, H.-K. Mao, and R. J. Hemley, Phys. Rev. B **70**, 174107 (2004).

¹² L. W. Bruch and I. J. McGee, J. Chem. Phys. **59**, 409 (1973).

¹³ M. J. Cohen and J. Murrel, Chem. Phys. Lett. **260**, 371 (1996).

¹⁴ P. Loubeyre, Phys. Rev. Lett. **58**, 1857 (1986).

¹⁵ S.-Y. Chang and M. Boninsegni, J. Chem. Phys. **115**, 2629 (2001).

¹⁶ C. P. Herrero, J. Phys.:Condens. Matter. **18**, 3469 (2006).

¹⁷ C.-L. Tian, F.-S. Liu, F.-Q. Jing, and L.-C. Cai, J. Phys.:Condens. Matter. **18**, 8103 (2006).

¹⁸ A. Grechnev, S. M. Tretyak, Y. A. Freiman, A. F. Goncharov, and E. Gregoryanz, Phys. Rev. B **92**, 024102 (2015).

¹⁹ S. Grimme, J. Comp. Chem. **27**, 1787 (2006).

²⁰ K. Berland, V. R. Cooper, K. Lee, E. Schröder, T. Thonhauser, P. Hyldgaard, and B. I. Lundqvist, Rep. Prog. Phys. **78**, 066501 (2015).

²¹ C. Cazorla, Coord. Chem. Rev. **300**, 142 (2015).

²² W. Cencek, M. Jeziorska, O. Akin-Ojo, and K. Szalewicz, J. Phys. Chem. A **111**, 11311 (2007).

²³ W. Cencek, K. Patkowski, and K. Szalewicz, J. Chem. Phys. **131**, 064105 (2009).

²⁴ J. P. Perdew, K. Burke, and M. Ernzerhof, Phys. Rev. Lett. **77**, 3865 (1996).

²⁵ G. Kresse and J. Fürthmüller, Phys. Rev. B **54**, 11169 (1996).

²⁶ P. E. Blöchl, Phys. Rev. B **50**, 17953 (1994).

²⁷ G. Kresse and D. Joubert, Phys. Rev. B **59**, 1758 (1999).

²⁸ C. Cazorla, M. J. Gillan, S. Taioli, and D. Alfè, J. Chem. Phys. **126**, 194502 (2007).

²⁹ S. Taioli, M. J. Gillan, C. Cazorla, and D. Alfè, Phys. Rev. B **75**, 214103 (2007).

³⁰ C. Cazorla and J. Íñiguez, Phys. Rev. B **88**, 214430 (2013).

³¹ S. A. Shevlin, C. Cazorla, and Z. X. Guo, J. Phys. Chem. C **116**, 13488 (2012).

³² C. Cazorla, D. Alfè, and M. J. Gillan, Phys. Rev. Lett. **101**, 049601 (2008).

³³ D. Alfè, Comp. Phys. Commun. **180**, 2622 (2009).

³⁴ C. Cazorla, G. Astrakharchick, J. Casulleras, and J. Boronat, New Journal of Phys. **11**, 013047 (2009).

³⁵ C. Cazorla and J. Boronat, Phys. Rev. B **77**, 024310 (2008).

³⁶ C. Cazorla, G. Astrakharchick, J. Casulleras, and J. Boronat, J. Phys.: Condens. Matter **22**, 165402 (2010).

³⁷ M. C. Gordillo, C. Cazorla, and J. Boronat, Phys. Rev. B **83**, 121406(R) (2011).

³⁸ S. A. Chin, Phys. Rev. A **42**, 6991 (1990).

³⁹ C. Cazorla, Y. Lutsyshyn, and J. Boronat, Phys. Rev. B **85**, 024101 (2012).

⁴⁰ C. Cazorla, Y. Lutsyshyn, and J. Boronat, Phys. Rev. B **87**, 214522 (2013).

⁴¹ R. Rota, Y. Lutsyshyn, C. Cazorla, and J. Boronat, J. Low Temp. Phys. **168**, 150 (2012).

⁴² F. Ercolessi and J. B. Adams, Europhys. Lett. **26**, 583 (1994).

⁴³ J. Sala, E. Guàrdia, J. Martí, D. Spångberg, and M. Masia, J. Chem. Phys. **136**, 054103 (2012).

⁴⁴ M. Masia, E. Guàrdia, and P. Nicolini, Int. J. Quantum. Chem. **114**, 1036 (2014).

⁴⁵ J. Nocedal and S. J. Wright, *Numerical Optimization* (Springer, Berlin, 2006).

⁴⁶ P. Loubeyre, R. LeToullec, J. P. Pinceaux, H. K. Mao, J. Hu, and R. J. Hemley, Phys. Rev. Lett. **71**, 2272 (1993).

⁴⁷ F. Birch, J. Geophys. Res. **83**, 1257 (1978).

⁴⁸ C. Cazorla, D. Errandonea, and E. Sola, Phys. Rev. B **80**, 064105 (2009).

⁴⁹ R. Barnett, P. Reynolds, and W. A. Lester Jr., J. Comput. Phys. **96**, 258 (1991).

⁵⁰ J. Casulleras and J. Boronat, Phys. Rev. B **52**, 3654 (1995).

⁵¹ G. Geneste, M. Torrent, F. Bottin, and P. Loubeyre, Phys. Rev. Lett. **109**, 155303 (2012).

- ⁵² J. M. McMahon, M. A. Morales, C. Pierleoni, and D. M. Ceperley, *Rev. Mod. Phys.* **84**, 1607 (2012).
- ⁵³ M. A. Morales, J. M. McMahon, C. Pierleoni, and D. M. Ceperley, *Phys. Rev. B* **87**, 184107 (2013).
- ⁵⁴ F. Datchi, S. Ninet, M. Gauthier, A. M. Saitta, B. Canny, and F. Decremps, *Phys. Rev. B* **73**, 174111 (2006).
- ⁵⁵ C. J. Pickard and R. J. Needs, *Nature Materials* **7**, 775 (2008).
- ⁵⁶ I. Errea, B. Rousseau, and A. Bergara, *Phys. Rev. Lett.* **106**, 165501 (2011).
- ⁵⁷ Y. Feng, J. Chen, D. Alfè, X-Z. Li, and E. Wang, *J. Chem. Phys.* **142**, 064506 (2015).
- ⁵⁸ D. A. Arms, R. S. Shah, and R. O. Simmons, *Phys. Rev. B* **67**, 094303 (2003).
- ⁵⁹ G. V. Sin'ko and N. A. Smirnov, *J. Phys.: Condens. Matter* **14**, 6989 (2002).
- ⁶⁰ G. Grimvall *et al.*, *Rev. Mod. Phys.* **84**, 945 (2012).
- ⁶¹ E. J. L. Borda, W. Cai, and M. de Koning, *Phys. Rev. Lett.* **112**, 155303 (2014).